Journal of Hydrology 544 (2017) 125–132

Contents lists available at ScienceDirect

Journal of Hydrology

journal homepage: www.elsevier.com/locate/jhydrol

Research papers

Adsorption and retarded diffusion of Eu^{III}-$EDTA^{-}$ through hard clay rock

Michael Descostes [a,1], Ingmar Pointeau [a,2], Jean Radwan [a], Jenna Poonoosamy [a,3], Jean-Luc Lacour [b], Denis Menut [b,4], Thomas Vercouter [b], Romain V.H. Dagnelie [a,*]

[a] DEN-Service d'Etude du Comportement des Radionucléides (SECR), CEA, Université Paris-Saclay, F-91191 Gif-sur-Yvette, France
[b] DEN-Service d'Etudes Analytiques et de Réactivité des Surfaces (SEARS), CEA, Université Paris-Saclay, F-91191 Gif-sur-Yvette, France

ARTICLE INFO

Article history:
Received 16 February 2016
Received in revised form 22 September 2016
Accepted 9 November 2016
Available online 15 November 2016
This manuscript was handled by L. Charlet, Editor-in-Chief, with the assistance of Christophe Tournassat, Associate Editor

Keywords:
Europium
EDTA
Organic
Diffusion
Adsorption
Clay rock

ABSTRACT

Adsorption and diffusion experiments of Eu^{III} were performed in Callovo-Oxfordian (COx) clay rock in the presence of EDTA. The predictive model based on binary system parameters (Eu/COx and EDTA/COx) was in good agreement with the results for the Eu/EDTA/COx ternary system. At low EDTA concentrations, the behaviour of Eu^{III} was mainly driven by Eu^{3+}adsorption and complexation by carbonates and EDTA. At higher EDTA concentrations, the behaviour of Eu^{III} was driven by the adsorption of $[Eu^{III}\text{-EDTA}]^{-}$ anions. Europium was then used as a probe to estimate the transport of EDTA. Three through-diffusion experiments of EDTA were compared with 14C, Eu and 152Eu tracers. Eu^{III}-EDTA was not quantitatively dissociated by diffusion through the rock. The effective diffusion coefficients quantified $D_e(Eu^{III}\text{-EDTA}) = 1.5\text{–}1.7 \cdot 10^{12}\ m^2\ s^{-1}$ were an order of magnitude lower than that of water, evidencing the anionic exclusion of $[Eu^{III}\text{-EDTA}]^{-}$ within the clay rock. Break-through curves and diffusion profiles confirmed retardation due to significant adsorption on the clay rock ($R_d(Eu^{III}\text{-EDTA}) \sim 6\text{–}14\ L\ kg^{-1}$) in comparison with inorganic anions. However, the model based on batch adsorption measurements failed to predict the diffusion results. All experiments displayed an early break-through of EDTA complexes. This behaviour contrasted with results on iron oxides rich sediments, which usually led to higher retardation than expected from the batch studies.

1. Introduction

The fate of metals and radionuclides in the environment is essentially governed by adsorption processes on mineral surfaces and aqueous complexation (Hummel, 2008). Metals are commonly trapped by adsorption on minerals with high cationic exchange capacities such as clays. This adsorption can be modified in the presence of aqueous complexing ligands. Inorganic and organic ligands are known to increase metal solubility and decrease adsorption by reducing the concentration of free cations in solution. Among the latter, phthalic acids and esters are frequently used as additives in plastics and released into the geosphere from waste. Chelating agents such as EDTA, NTA and DTPA are also used for their complexing properties in the medical and textile industries, as well as being used to extract rare earth elements (Xie et al., 2014). Despite numerous studies dedicated to the transport organic molecules in sedimentary rocks and aquifers, transport parameters are hardly predictable in natural heterogeneous samples (Borisover and Davis, 2015; Schaffer and Licha, 2015). Up to now, however, migration measurements remain crucial for assessing the transport of anthropogenic organic species. This paper focuses on the transport of ethylenediaminetetracetic metallic complexes (Metal-EDTA) in hard, sedimentary clay rocks. The results are discussed with emphasis on a comparison between the adsorption data on crushed rock and retarded diffusion in compact rock.

There is an extensive bibliography on the effect of EDTA on cation migration. For instance, it is worth citing: adsorption of Zn^{II}-Pb^{II}/EDTA on clay (Darban et al., 2000); transport of $^{241}Am^{3+}$, $^{60}Co^{2+}$, $^{137}Cs^{+}$ and $^{85}Sr^{2+}$ in the presence of EDTA through sand/silt/clay soils (Pace et al., 2007; Seliman et al., 2010); mobility of Th^{IV}-EDTA through sand (Reinoso-Maset et al., 2012). The adsorption-dissociation of $Co^{II/III}$-EDTA during transport has also been reported to occur on iron oxide-coated sand (Szecsody et al., 1994, 1998), on Ferrihydrite (Brooks et al., 1996), and on saprolite (Mayes et al., 2000; Gwo et al., 2007). More recently, a

* Corresponding author.
E-mail address: romain.dagnelie@cea.fr (R.V.H. Dagnelie).
[1] Address: AREVA Mines, R&D Department, F-92084 Paris la Défense, France.
[2] Address: DEN-Service d'Exploitation, d'Expertise et de Caractérisation (SEEC), CEA Cadarache, F-13108 Saint Paul lez Durance, France.
[3] Address: Forschungszentrum Juelich GmbH, 52425 Juelich, Deutschland.
[4] Address: DEN-Service des Recherches Métallurgiques Appliquées (SRMA), CEA, Université Paris-Saclay, F-91191 Gif-sur-Yvette, France.

http://dx.doi.org/10.1016/j.jhydrol.2016.11.014
0022-1694/

diffusion experiment of ^{14}C-EDTA was performed through Callovo-Oxfordian (COx) clay rock (Dagnelie et al., 2014). This rock was largely investigated by the French nuclear radioactive waste management agency (Andra, 2005). A lower diffusivity of EDTA than non-ionic species indicated the anionic exclusion from pore surfaces despite a significant affinity measured by batch ($R_d \sim 6.5$ L kg^{-1}). A striking result was the much lower K_d value measured during the diffusion experiments (<0.1 L kg^{-1}) than that given in past data. This manuscript uses the notation R_d for batch adsorption experiments, which provide us with a distribution ratio. This ratio is only interpreted as an adsorption coefficient, K_d, assuming the reversibility of the process as in the case of through-diffusion experiments. This "early break-through", i.e. $K_d < R_d$, is typical in organic molecule/soil systems (Pignatello and Xing, 1996). However, the opposite behaviour was reported for Co^{II}-EDTA and Sr^{II}-EDTA percolation through sediments ($K_d > R_d$ in Szecsody et al., 1998 and Pace et al., 2007). This paper discusses experiments that were performed with other M-EDTA complexes so as to strengthen the retardation factor expected in COx clay rock. This is why we have focused on the [Eu^{III}-EDTA]$^-$ diffusion.

We chose Eu because its adsorption on various clayey minerals, oxides and cementitious materials in the presence of organic matter is well documented. It is worth mentioning, for example, (i) Eu/NOM adsorption on illite (Bruggeman et al., 2010), (ii) in situ experiments on natural sediments (Kaplan et al., 2010), (iii) Eu/organic co-contaminants on smectite (Bauer et al., 2005), (iv) Eu/acetic, oxalic and carbonic acids or fulvic acids on α-alumina (Alliot et al., 2006; Wang et al., 2000), and (v) Eu/Isa and gluconic acids on calcite (Tits et al., 2005). All these studies reveal that the adsorption of europium is governed by the concentration of free cations in solution, which decreased in the presence of ligands. To our knowledge, no study has been dedicated to higher concentrations of ligands causing the behaviour of Eu to be governed by its organic complex. Since this approach has been successfully applied to cobalt and strontium EDTA complexes, we used Eu as a probe to assess EDTA transport. A key issue of this work was to evaluate if metal-EDTA species would display similar early break-though than ^{14}C-EDTA in COx clay rock. By way of conclusion, we discuss the predictability of diffusion models based on adsorption data measured on crushed rock.

2. Material and methods

2.1. Clay rock and chemicals

Two types of experiments were performed in this study: adsorption in batches on crushed rock and through-diffusion in hard rock. Experiments were carried out on a drillcore sample from the COx clay rock formation taken from −500.8 to −501.0 m in depth (C2b1 layer). Samples were composed of clayey minerals (∼35 ± 5%), carbonates (∼28 ± 3%), quartz (∼27 ± 5%) and other minor phases: potassic feldspars or siderite (<3%), and pyrite or organic matter (<1%) (Gaucher et al., 2004). Deep argillaceous rocks are reducing environments ($E_H \sim -0.2$ V) which is why the samples were protected from O_2 in an anoxic glove box. Each core was sliced into 10 mm-thick pieces perpendicular to the bedding, and then cut into discs of 35 mm in diameter. The remaining rock was ground to fine powder (<63 μm) and equilibrated with synthetic porewater before the adsorption experiments. The composition of the synthetic porewater is given in Table S1. Solutions were prepared with salts of high purity (>99%). Gaseous nitrogen with CO_2 ($pCO_2 \sim 10^{1.9}$ atm) was bubbled for 1 h and the pH was checked to be equal to 7.2 ± 0.2. Solutions of organic complex were obtained by adding high-purity $Na_2H_2EDTA{\cdot}2H_2O$ and $Eu_2(SO_4)_3$ salts and the pH was adjusted with fresh NaOH solution. The radiolabelled tracers were ^{14}C-EDTA (Sigma 30,471-9) and $^{152}EuCl_3$ (CERCA LEA, 6.8 MBq.g^{-1} in HCl 1 M).

2.2. Adsorption experiments

Adsorption isotherms of ^{14}C-EDTA and ^{152}Eu were first performed to quantify the adsorption properties of the sample (EDTA/COx and Eu/COx binary system). The adsorption of ^{152}Eu in the presence of EDTA (Eu/EDTA/COx ternary system) was then measured and compared with predictive modelling. The experiments followed a protocol adapted from Descostes and Tevissen (2004). Clay powder was rinsed under anoxic conditions (m/V = 0.25 g mL^{-1}) with synthetic porewater (Table S1). After 24–48 h of agitation, the tubes were centrifuged at 10,000*g* for 30 min and supernatant was renewed. This operation was repeated four times to equilibrate the clay mineral. Adsorption experiments were then carried out at 21 °C with a mean solid/liquid ratio of 0.011 g mL^{-1} and 0.05 g mL^{-1} for europium and EDTA adsorption respectively. Adsorption started when the EDTA solution and the ^{14}C-EDTA or ^{152}Eu radiotracer were introduced and the tubes were agitated. An initial concentration was fixed for the Eu/EDTA/COx ternary system: $[Eu]_0 \sim 10^{-9}$ mol L^{-1}. Measurements were performed after centrifugation (50,000 g for 1 h). Supernatant solutions were weighed and measured by γ counting (Packard 1480 WIZARD 3) for ^{152}Eu, or by liquid scintillation counting for ^{14}C (Packard TRICARB 2500, ultima gold™). The solid-to-liquid distribution ratio, R_d (L kg^{-1}), was estimated using the following equation:

$$R_d(t) = \frac{[X]_{sorbed}}{[X]_{residual}} = \left(\frac{C_0}{C(t)} - 1\right) \times \frac{V}{m} = f([EDTA]) \quad (1)$$

where X represents EDTA or Eu, C the concentration (mol L^{-1}), V (mL) the solution volume, and m (g), the dry mass of the clay rock.

2.3. Diffusion experiments

Two through-diffusion experiments were performed with Eu-EDTA, namely runs B and C. The results of these runs were compared with previously published data (i.e. run A) using ^{14}C-EDTA (Dagnelie et al., 2014). The characteristics of the experiments are summarised in Table 1. Radioactive ^{152}Eu was used in run B to assess retardation at trace concentrations ($2.1 \cdot 10^{-7}$ mol L^{-1}). Concurrently, stable europium was used in run C ($1.0\ 10^{-4}$ mol L^{-1}) to assess the concentration effect. The experimental set-up is described in detail elsewhere (Bazer-Bachi et al., 2006, 2007). Briefly, the through-diffusion cells comprised upstream and downstream reservoirs, with volumes of 175 and 125 mL respectively. Rock disks were pasted between two filterplates inside the diffusion cells. After equilibration, the upstream solution was replaced by a fresh poral solution containing $2.7 \cdot 10^{-2}$ mol L^{-1} of EDTA and a tracer. Experiments were kept in a temperature-controlled room (21 ± 1 °C). Both compartments were periodically sampled. Removed volumes were renewed with the initial solution. Tracers were measured by α–β liquid scintillation counting for run A, γ counting for run B and inductively coupled plasma mass spectrometry (ICP-MS 810-MS VARIAN) for run C.

2.4. Time-resolved laser-induced fluorescence spectroscopy (TRLFS)

The stability or dissociation of the Eu^{III}-EDTA complex was evaluated after diffusion. For this reason, the speciation of Eu^{III} was determined by time-resolved laser-induced fluorescence spectroscopy (TRLFS). Upstream and downstream solutions were analysed before and after diffusion experiments. Results were compared with a reference containing [Eu-EDTA]$^-$ and a MES

Table 1
Composition of solutions in upstream compartments of through-diffusion cells.

Run	Duration (days)	Tracer	$[EDTA]_{tot}$ (mol L^{-1})	$A_0(^{14}C)$ (MBq)	$[Eu]_{tot}$ (mol L^{-1})	$A_0(^{152}Eu)$ (MBq)
A	450	^{14}C-EDTA	$2.7 \cdot 10^{-2}$	0.89648	0	0
B	750	^{152}Eu	$2.7 \cdot 10^{-2}$	0	$2.1 \cdot 10^{-7}$	0.98563
C	710	Eu	$2.7 \cdot 10^{-2}$	0	$1.0 \cdot 10^{-4}$	0

buffering agent (pH 6) in water. Europium was excited with a tunable OPO laser at 396 nm, providing 1 mJ per pulse at 10 Hz for a period of 5 ns. The spectrometer was a monochromator spectrograph (Acton 2358i) with a 600-groove/mm diffraction grating (500-nm blaze, iCCD-PIMAX camera). The delay and width of the acquisition gate were set to values that maximised the fluorescence signal. The fluorescence of Eu after excitation at 396 nm was collected at right angle to the laser beam between 560 and 640 nm.

2.5. Micro-laser-induced breakdown spectroscopy (LIBS-micro probe)

Quantification of europium in the rock also gave us information on adsorption. There are specific techniques to quantify the Eu profile in hard rocks, such as Rutherford backscattering spectrometry (RBS, Alonso et al., 2009) or micro-laser-induced breakdown spectroscopy (LIBS-micro probe, Menut et al., 2003, 2005). The quantitative mapping of the Eu profile inside the rock was provided by a LIBS-micro probe after run C. The rock disc was cut after diffusion (t = 888 days) into 3 mm thick slices (geometry detailed in Fig. S1 of the Supplementary material). The size of slices was $dX \times dZ = 10 \times 35$ mm^2 (X being the diffusion direction). Two Eu maps are reported herein to illustrate the reproducibility of the technique. The maps, namely C1 and C2, correspond to the slices located at y = 0 ± 1.5 and y = 6 ± 1.5 mm from the centre of the disc. The resolution of the laser spot gave an average of 1000 measurements per profile (dX = 10 mm). A few dozen profiles were performed along dz ~ 1 mm per map. The experimental set-up was detailed in the document by Menut et al. (2003). A Nd-YAG laser (Minilite II Continuum) operating at 266 nm with an energy of 4 mJ per pulse was used as the ablation source. By using a diaphragm, the spatial resolution was around 10 μm, which thereby decreased the interaction energy to ~25 μJ. Europium was measured at 462.72 nm by a CCD camera.

Europium maps were calibrated by estimating the total quantity of Eu in rock samples. For this reason, a small amount of clay was drilled from X = 280–940 μm. The corresponding sample was weighed and then entirely dissolved in a Teflon beaker with a leaching solution made of aqua regia and HF. The solution was then filtered and the total Eu concentration was measured by ICP-MS.

3. Calculation

3.1. Adsorption modelling

The adsorption of both cations and organic anions on clay rock was adjusted by a Langmuir-type multisite model. The adsorption properties (sites densities and affinities) of the clay rock sample were adjusted on the Eu/COx and EDTA/COx binary systems. The behaviour of the Eu/EDTA/COx ternary system was then predicted on the basis of previous data and the aqueous speciation. Speciation calculations were performed with PhreeqC (V.2.18, Parkhurst and Appelo, 1999) and the thermodynamic database provided by Andra, *ThermoChimie* TDB V9 (Giffaut et al., 2014). One missing complexation constant, $\beta°[Eu\text{-}EDTA]^-$ was extrapolated from Wu and Horrocks (1996). The comparison between the predicted and experimental adsorption isotherm, $K_d(Eu/COx) = f[EDTA]$, is discussed in Section 4.

3.2. Diffusion modelling

The analysis of the through-diffusion results is based on Fick's second law (Crank, 1975):

$$\frac{\partial C}{\partial t} = \frac{D_e}{\varepsilon_a + \rho_g(1-\varepsilon_a)K_d}\frac{\partial^2 C}{\partial x^2} = \frac{D_e}{\varepsilon_a \times R} = \frac{D_e}{\alpha}\frac{\partial^2 C}{\partial x^2} \quad (2)$$

with C representing the concentration (mol m^{-3}), t the time (s), D_e the effective diffusion coefficient (m^2 s^{-1}), ε_a the diffusion-accessible porosity, ρ_g the grain density (~2.7 kg L^{-1}), K_d the adsorption coefficient, and α the rock capacity factor. $R = \alpha/\varepsilon_a$ is called retardation factor. The initial conditions were $C(x = 0) = C_0$, $C(x \neq 0) = 0$. Two methods were compared to solve the diffusion equation. Firstly, reactive transport modelling was performed using PhreeqC. In this case, the retarded diffusion of EDTA and Eu were predicted using the adsorption parameters obtained from batch experiments. In the first case, the same effective diffusion coefficient was assumed for both the EDTA and Eu^{III}-EDTA species and adjusted to $D_e = 1.5\ 10^{-12}$ m^2 s^{-1}. Secondly, fully analytical solutions were performed to fit the results with a constant K_d value. The resolution was performed in the Laplace space (Moridis, 1998). In the second case, two parameters (D_e, α) were adjusted. They are reported in Table 3. Adjustment was performed by the least-square fitting of experimental and modelled results with a weighting inversely proportional to the experimental precision. A simultaneous fit on both the downstream flux and the upstream concentration was performed. The downstream flux, J (moles m^{-2} s^{-1}) was defined by Eq. (3):

$$J_{down}(t) = \frac{dn_{down}(t)}{S \times dt} = \frac{V_{down}}{S}\lim_{\Delta t \to 0}\frac{C_{down}(t+\Delta t) - C_{down}(t-\Delta t)}{2 \times \Delta t} \quad (3)$$

where n_{down} is the amount of molecules in the downstream compartment in (moles), V_{down} the downstream volume, S the sample surface, and Δt the duration between two successive measurements. The results are discussed on the basis of a normalised flux:

$$^{NORM}J_{down}(t) = \frac{L}{C_0}J_{down}(t) \quad (4)$$

with L (m) being the sample width and C_0 (moles m^{-3}) the initial concentration. By using $^{NORM}J_{down}$ (m^2 s^{-1}), the direct comparison of the different experiments was possible, regardless of C_0 or L. Moreover, diffusion cells tend to move towards a stationary state where the flux is proportional to the effective diffusion coefficient as described by Eq. (5).

$$J_{down}(t \to \infty) = \frac{D_e \times (C_{up} - C_{down})}{L} \quad ^{NORM}J_{down}(t \to \infty) \approx D_e \quad (5)$$

If the upstream and downstream concentrations evolve slowly, $(C_{up}\text{-}C_{down}) \sim C_0$, the normalised flux rises to a plateau with a value close to the effective diffusion coefficient. Experimental determination of this plateau is relevant since it estimates D_e independently of the porosity and the adsorption process.

4. Results

4.1. Adsorption of Eu^{III}-EDTA on clay rock

Fig. 1 and Table 2 report the adsorption isotherms and parameters adjusted from the binary systems. A two-site ($S_1 + S_2$) Langmuir model was adjusted with the Eu/COx adsorption isotherm. A single site (S_O) was considered for the EDTA/COx adsorption isotherm with a constant affinity of all EDTA species. Such a rough assumption supposes that the adsorption of EDTA complexes might only be scarcely affected by the cation inside the complex (Tebes-Stevens et al., 1998). The value R_d(EDTA/14 days) = 13.6 ± 2.3 L kg^{-1} was slightly higher than that reported in previous data (Dagnelie et al., 2014).

Adsorption on the ternary system was then predicted using the previous data adjusted to binary systems. The adsorption isotherm of europium was measured as a function of [EDTA] (Fig. 2). The results were in very good agreement with the predictive model. The adsorption of europium is constant at the lowest concentration, with a value R_d^{MAX}(Eu) between $8.2 \cdot 10^4$ and $1.7 \cdot 10^5$ L kg^{-1}. These values are close to the available published results (Rabung et al., 2005; Tertre et al., 2006), considering clayey minerals as the major adsorbing phases (in our case 21% of illite, 11 ± 2% of interstratified illite/smectite considering CEC). Europium mainly remains in cationic form $[Eu(CO_3)]^+$ (Fig. 2, bottom). At intermediate concentrations, $10^{-6} < [EDTA] < 10^{-3}$ mol L^{-1}, the adsorption of Eu decreases. Anionic species become prevalent and display a lower adsorption than cations. The corresponding complexation reaction is:

$$[Eu - CO_3]^+ + [Ca - EDTA]^{-2} = [Eu - EDTA]^- + Ca^{2+} + CO_3^{2-} \quad (6)$$

It is worth highlight the fact that the EDTA concentration range required to decrease R_d(Eu) is correctly predicted by the model, confirming the thermodynamic data listed in Table 2. Above [EDTA] > 10^{-3} mol L^{-1}, R_d(Eu) reached a plateau with a value close to the sole complexing agent EDTA. The adsorption of $[Eu^{III}\text{-EDTA}]^-$ was driven by the anionic complex adsorption.

An important feature was the saturation of adsorption sites above [EDTA] > 10^{-2} mol L^{-1} which was more pronounced for EDTA (Fig. 1) than for Eu^{TOT} (Fig. 2). When the EDTA concentration increases, the saturation of adsorption sites leads to Langmuir-type isotherms for EDTA. Concerning the adsorption of Eu^{TOT}, two antagonist effects occur when the concentration of EDTA increases. Firstly, the saturation of surfaces decreases the adsorption of Eu-EDTA in similar proportions to EDTA since they display similar affinities for adsorbing sites. In the meantime, however, the EDTA/Eu^{TOT} ratio increases, as well as for Eu-EDTA/Eu^{TOT} and thus $R_d(Eu^{TOT})$. This explains why the saturation effects were less pronounced for Eu^{TOT} than for EDTA. Thanks to this feature, the use of Eu as a probe has the advantage to assessing the diffusion of EDTA complexes with minimised saturation effects.

4.2. Through-diffusion of Eu^{III}-EDTA

4.2.1. Eu speciation measured by TRLFS

TRLFS measurements were performed to assess the speciation and stability of Eu^{III}-EDTA. The interaction of EDTA with minerals potentially dissociates complexes by releasing trace elements such as Fe^{III}, Al^{III}. For example, the adsorption-dissociation of $Co^{II/III}$-EDTA into Fe^{III}-EDTA was largely studied during percolation through iron oxide-coated sand (Szecsody et al., 1994, 1998). However, COx clay rock only shows a low amount of iron, mainly in a reduced state ($Fe^{II}S_2$, $Fe^{II}CO_3$). The slow Eu^{III}-EDTA dissociation in COx clay was only evidenced at high solid/solution ratios in Dagnelie et al. (2015). In the present experimental set-up,

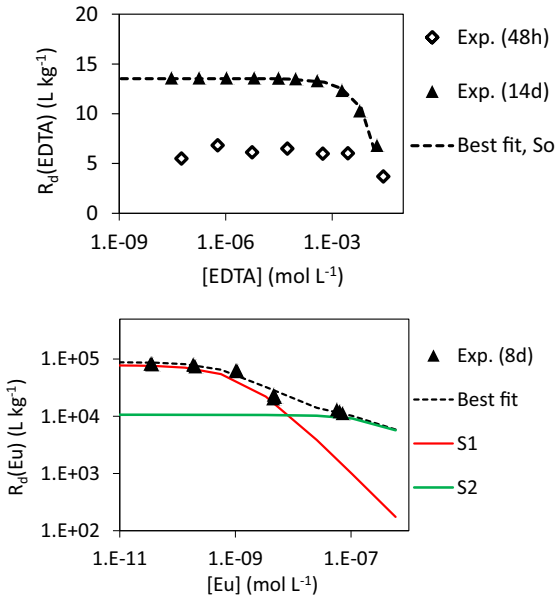

Fig. 1. Adsorption isotherms on the binary systems used for parameter fitting. (top) Langmuir isotherm of EDTA on COx clay rock at 14 days adjusted with 1 site (So), (bottom) Adsorption isotherm of Eu on COx clay rock at 8 days adjusted with 2 sites (S_1 & S_2).

Table 2
Data used for adsorption modelling. Bold characters are adjusted parameters. Adsorption sites for cations ($S_1 + S_2$) are initially saturated by an inert cation noted T^{3+}. The adsorption site for organic anions (S_O) displays identical affinity for all EDTA complexes. Complexation constants are taken from Andra database (*Thermochimie* TDB V9, available in https://www.thermochimie-tdb.com/).

Surface complexation reaction	Site capacity (moles kg(COx)$^{-1}$)	Affinity (log K)
S_1-OT + Eu^{3+} = S_1-O-Eu + T^{3+}	**$1.04 \cdot 10^{-4}$**	**7.92**
S_2-OT + Eu^{3+} = S_2-O-Eu + T^{3+}	**$7.4 \cdot 10^{-3}$**	**5.2**
S_O + $[M\text{-EDTA}]^{Y-}$ = S_O-$[M\text{-EDTA}]^{Y-}$	**$4.0 \cdot 10^{-1}$**	**1.93**
Complexation constants	Reference	(log β°)
Eu^{3+} + $EDTA^{4-}$ = $[Eu\text{-EDTA}]^-$	Wu & Horrocks	17.52
	(*β° extrapolated*)	*19.15*
Eu^{3+} + CO_3^{2-} = $[Eu\text{-}CO_3]^+$	Andra TDB V9	7.9
Eu^{3+} + 2 CO_3^{2-} = $[Eu(CO_3)_2]^-$	Andra TDB V9	12.9
Eu^{3+} + SO_4^{2-} = $[Eu\text{-}SO_4]^+$	Andra TDB V9	3.5
Ca^{2+} + $EDTA^{4-}$ = $[Ca\text{-EDTA}]^{2-}$	Andra TDB V9	12.69

Eu^{III}-EDTA dissociation was expected to be slow and the complex was expected to remain both stable and in a sufficient amount to be measured. This was confirmed by the fluorescence spectra of the upstream and downstream solution after through-diffusion (Fig. 3). The main features are the fluorescence bands centred at 580.6, 593.5 and 616.1 nm, corresponding to the transitions from the $^5D_0$ excited state to the $^7F_0$, $^7F_1$, and $^7F_2$ ground levels respectively. The four measurements present similar spectra with respect to the positions and shape of the fluorescence bands. Europium mainly remained in $[Eu^{III}\text{-EDTA}]^-$ form and was not quantitatively dissociated during the experiment. The labile fraction of Eu^{TOT} was dominated by the Eu^{III}-EDTA complex and Eu^{3+} adsorption remained negligible compared with that of Eu^{III}-EDTA in our system.

4.2.2. Downstream flux and upstream concentration

The results of the through-diffusion experiments are shown in Fig. 4. An early break-through of tracers was observed in all the three runs. Neither EDTA nor Eu were expected to be measurable

Table 3
Characteristics of transport parameters of EDTA complexes in COx clay rock. Distribution ratio, R_d, measured by batch and K_d values extrapolated from diffusion experiments. Bold characters are best-fit parameters. Min/max values between brackets show the visual uncertainties represented in Figs. 4 and 5. Italic characters are additional adjustments performed on the curve written in superscript.

		Mock-Up[a]		Run A[b]	Run B	Run C
Species		EDTA Fe-EDTA	Eu^{III}-EDTA	^{14}C-EDTA	Eu^{III}-EDTA	Eu^{III}-EDTA
Diffusion through compact rock	V/m (L kg^{-1})	4.10^{-3}		5–7		
	D_e (10^{-12} m^2 s^{-1})	3.9	0.17	**0.94** [0.7–1.3]	**1.7** [1.4–2.1]	**1.5** [1.3–1.7] *[0.4–1.7]^{LIBS}*
	α	9.0	13.5	**0.27** [0.20–0.35]	**7.5** [6–11]	**4.3** [3.6–4.8]
	K_d (L kg^{-1})	3.8	5.8	**0.08** *6.2^{UPSTREAM}*	**3.2**	**1.6** *[6.3–14]^{LIBS}*
Adsorption on crushed rock	R_d (L kg^{-1}) at lowest concentrations			6.2 (48 h)[a] **13.6** ± 3 (14 d)		
	R_d (L kg^{-1}) at [EDTA] = 2.7 10^{-2} mol L^{-1}			4.9 ± 2 (14 d)	4.4 (24 h) 16.0 ± 2 (8 months)	

[a,b] Taken from Dagnelie et al. (2014, 2015) respectively.

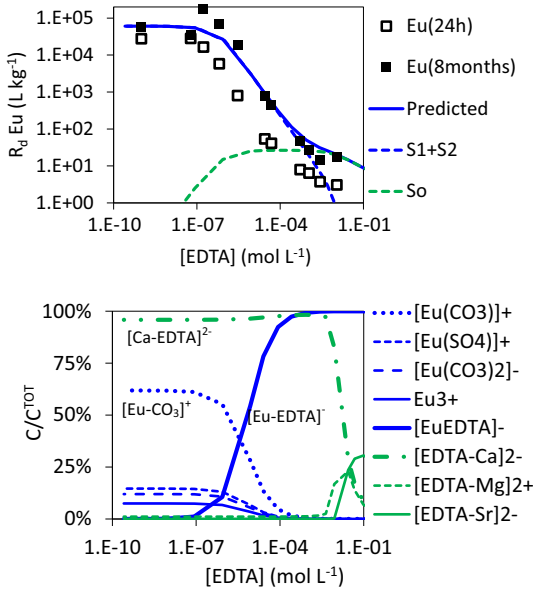

Fig. 2. Predictive modelling of the adsorption isotherm of the ternary system (Eu/EDTA/COx). (top) Adsorption of ^{152}Eu on COx clay rock as a function of [EDTA] $_{éq}$. ■/▲ Experimental data solid line: predictive model. Dashed lines: contributions of cations/anion-adsorbing sites ($S_1 + S_2/S_0$). (bottom) Speciation of europium and EDTA predicted in solution. ($[Eu]_0 \sim 10^{-9}$ mol L^{-1}) Blue/green lines show speciation of Eu/EDTA element in solution. (For interpretation of the references to colour in this figure legend, the reader is referred to the web version of this article.)

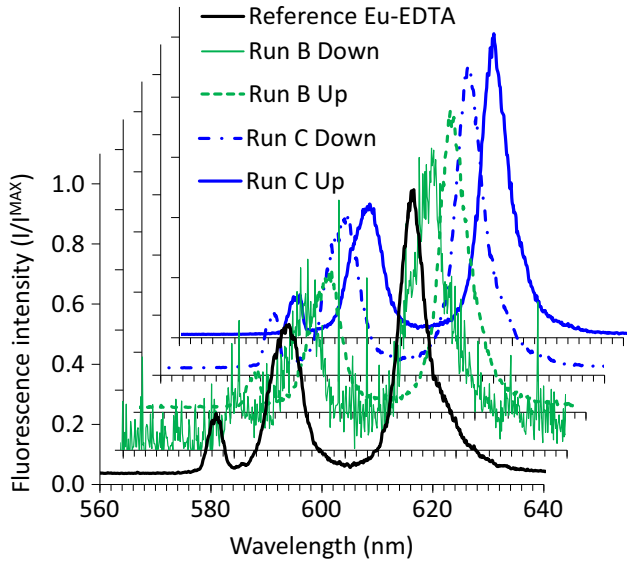

Fig. 3. Fluorescence spectra (TRLFS) of upstream and downstream solution in diffusion experiments; run B and C. Excitation wavelength at 396 nm.

in the downstream compartment according to the predictive model based on batch data (Fig. 4, the predicted downstream curves are not visible within 750 days; the black dotted line indicates the predicted upstream curve). The adjustment of two parameters (D_e, α) by using an analytical solution resulted in a semi-quantitative estimation of the EDTA complex adsorption (Fig. 4, solid lines). In the case of run C in particular, both the upstream and downstream concentrations were correctly reproduced with the single set of parameters (D_e, K_d) = ($1.5 \cdot 10^{-12}$ m^2 s^{-1}, 1.6 L kg^{-1}). This result secured a good mass-balance during the experiment and a better level of confidence for this data. All the adjusted parameters are summarised in Table 3. The effective diffusion coefficients $D_e([Eu^{III}\text{-EDTA}]^-)$ = $1.7 \cdot 10^{-12}$ and $1.5 \cdot 10^{12}$ m s^{-1} were obtained in agreement with previous results $D_e(^{14}\text{C-EDTA}) = 0.94 \cdot 10^{-12}$ m^2 s^{-1}. These low effective diffusion coefficients, compared with that of water (D_e(HTO) ~ 20–25 $\cdot 10^{-12}$ m^2 s^{-1}), indicated anionic exclusion from the clay rock as evidenced with inorganics anions by Descostes et al. (2008).

Concerning adsorption, the $K_d(Eu^{III}\text{-EDTA})$ values of 1.6 and 3.2 L kg^{-1} were extrapolated from the rock capacity factor α. These values were compared with the data obtained from the batch experiments taking into account the saturation of adsorption sites. For this purpose, we considered the Langmuir parameters (K, S) and a linear concentration profile through the rock. Thus, $R_d^{CELL} = S/C_0 \times \ln(1 + K \times C_0)$ gave a low estimate of the adsorption expected in diffusion cells based on the batch data, e.g.: the EDTA adsorption isotherm with R_d^{MAX} = 13.6 L kg^{-1} and C_0 = 27 mM led to R_d^{CELL} = 7.8 L kg^{-1} expected during through-diffusion experiment. R_d^{CELL} was two times higher than the experimental $K_d(Eu^{III}\text{-EDTA})$ values calculated from batch experiments. The adsorption of Eu was assessed by a third method, which was provided thanks to the Eu solid profiles.

4.2.3. Europium profile in the rock

The total europium concentration in clay rock (in ppm) was measured using the LIBS micro-probe technique. It was compared with the modelled europium poral concentration based on the following equation:

$$[Eu]^{TOT}(\text{ppm}) = 10^3 \times M(Eu) \times [Eu]_{poral} \times \left[\frac{\varepsilon}{(1-\varepsilon)\rho_g} + K_d\right] \quad (7)$$

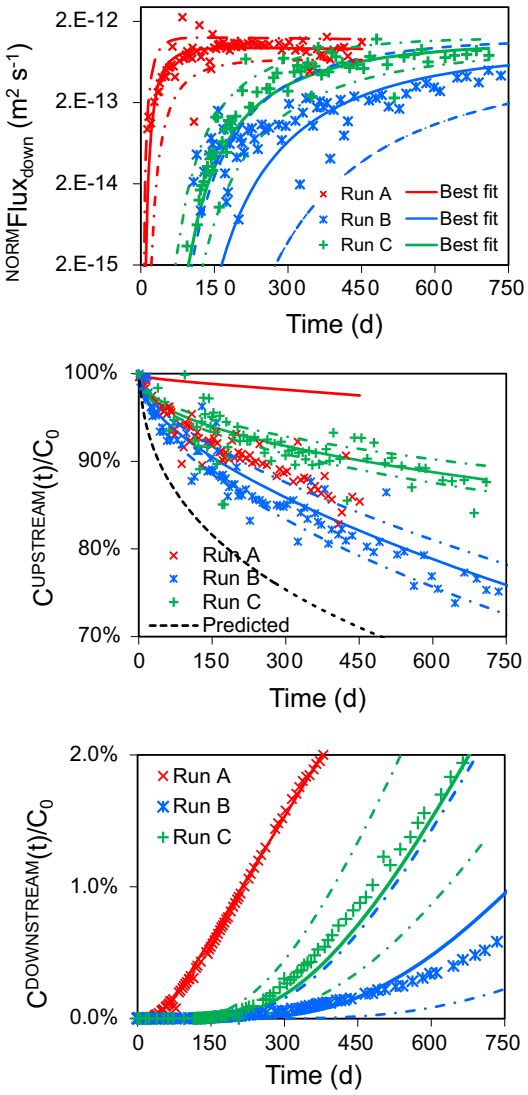

Fig. 4. Experimental (dot) and modelled data (line) from diffusion cells. Solid lines represent best fit and dotted lines are used to represent the visual estimation of uncertainties. (Top): Incoming daily flux in downstream compartment (normalised in $m^2\ s^{-1}$). (Middle) Concentration depletion in upstream reservoir. The black dashed line represents the predictive modelling of run C based on batch data. (Bottom) Concentration rise in downstream reservoir (normalised by $C_0^{UPSTREAM}$).

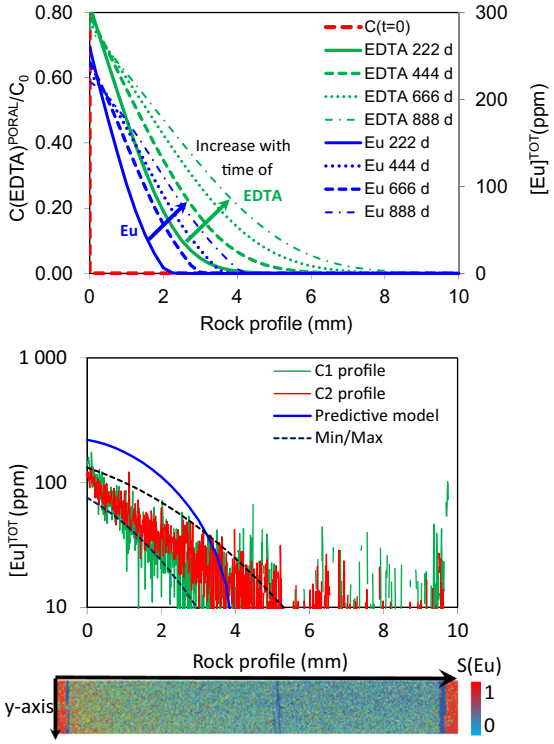

Fig. 5. (top) Temporal changes in Eu and EDTA profiles in the rock. Predictive model based on batch data (corresponding PhreeqC parameters in Table 2, $D_e = 1.5 \cdot 10^{-12}\ m^2\ s^{-1}$). (bottom) Comparison between Eu profiles measured in samples C1, C2, and predictive modelling (blue) Dashed lines corresponds to $D_e \in [0.4–1.7] \cdot 10^{-12}\ m^2\ s^{-1}$ and $K_d \in [6.3–14]\ L\ kg^{-1}$. (Bottom picture) Example of Europium mapping obtained on C2 sample. (For interpretation of the references to colour in this figure legend, the reader is referred to the web version of this article.)

5. Discussion

This section focuses on the confidence levels with respect to the transport parameters obtained and their applicability to other molecules or rocks.

5.1. Applicability of EDTA transport parameters

Table 3 gathers parameters which are representative of physical mass transfer of Eu^{III}-EDTA in COx clay rock. In all three diffusion runs, the normalised flux reached a quasi-stationary state. This provided an estimation of D_e(EDTA) independently of the adsorption process. Diffusion parameters of ^{14}CEDTA, EuEDTA and ^{152}EuEDTA were in good agreement: $D_e = 0.94/1.5/1.7 \cdot 10^{-12}\ m^2\ s^{-1}$. This reproducible result was representative of anionic exclusion and similar results should be expected for anionic complexes in COx and other clay-rich hard rocks.

Concerning adsorption on crushed rock, the model based on the (Eu/COx, EDTA/COx), binary systems predicted the experimental results on the Eu/EDTA/COx ternary system fairly well. At low EDTA concentrations, Eu is mainly driven by Eu^{3+} adsorption and complexation by carbonates and EDTA. Adsorption of the organic anions must be taken into consideration at high concentrations since it drives Eu^{III} behaviour. However, further experiments will be necessary to determine the solid phase(s) driving the adsorption of EDTA. Nonetheless, $R_d(Eu^{III}$-EDTA) may be estimated by analogy with other metal-EDTA complexes. Inner cations barely modified the complex affinity for surfaces. This methodology should suit other ternary systems composed of metal/chelating organic complexes/sedimentary rock.

Finally, the adsorption values measured by diffusion, K_d, differed slightly from batch data. Experiments B and C displayed early

where M(Eu) is the molecular mass of europium ($g\ mol^{-1}$). The temporal changes in Eu and EDTA predicted in the rock are illustrated in Fig. 5 (top). The results show that EDTA displays a lower retardation than Eu^{III}-EDTA due to the saturation of adsorption sites. Thus, the ratio [EDTA]/[Eu] is expected to increase along with the depth within the rock sample. This is in agreement with the constant speciation observed for $[Eu^{III}\text{-EDTA}]^-$.

The two europium profiles measured by LIBS-micro probe are shown in Fig. 5 (bottom). The Eu concentrations measured on the solid (upstream side) were $[Eu]^{TOT} = 120 \pm 15$ and 112 ± 10 ppm, see profiles C1 and C2 respectively. These results are lower than those calculated by the predictive model (220 ppm). Uncertainties on the D_e and K_d values were evaluated by a visual adjustment of the analytical model below and above experimental results (dotted lines). $D_e(Eu^{III}$-EDTA) fell in the range of $[0.4–1.7] \cdot 10^{-12}\ m^2\ s^{-1}$ in agreement with previous results. $K_d(Eu^{III}$-EDTA) was in the range of $[6.3–14]\ L\ kg^{-1}$, in the same range as the values expected from the adsorption isotherm.

break-through quantified by $R_d^{CELL}/K_d > 2$ for Eu^{III}-EDTA. This early break-through remains puzzling and hardly predictable for natural heterogeneous rocks. Yet similar trends were observed in COx clay rock for phthalate ($R_d^{CELL}/K_d \sim 5$, Dagnelie et al., 2014) and polymaleic acid ($R_d/K_d \sim 2$, Durce et al., 2014). It should be noted that the contrary behaviour, i.e. $R_d/K_d < 1$, was evidenced for EDTA complexes in other sedimentary rocks. Pace et al. (2007) studied the transport of Sr^{II}-EDTA in Hanford sediments while Szecsody et al. (1998) studied the transport of Co^{II}/Co^{III}-EDTA in subsurface sediments. In such cases, the oxidative dissociation of organic complexes by oxides created additional adsorption sites in column experiments. Furthermore, the dissolution of competing cations by EDTA inhibited adsorption in closed-batch systems. This bias between batch and diffusion experiments led to R_d/K_d ratios < 1 in iron oxide-containing sediments.

5.2. Origin of early break-through

This work confirmed and quantified the early break-through of metal-EDTA in COx clay rock. Such behaviour is typical of organic-soil interactions (Weber et al., 1991) and makes it difficult to predict the retardation of organic solutes (Roberts et al., 1986). The origin of this behaviour in COx clay rock remains to be evidenced. A few assumptions can be put forward: slow adsorption, chemical reactivity and adsorption site accessibility.

Slow adsorption induces early break-through during the transport of organic chemicals, especially for large-size humic acids (Pignatello and Xing, 1996). Similar cases were studied for EDTA-lanthanide complexes in Byegard et al. (2000) or for $Co^{II/III}$-EDTA reactive transport by Szecsody et al. (1994, 1998). In the latter case, the authors needed to modify a parameter from the batch dataset to model EDTA transport (adsorption rates, sites quantities). In our case, we quantified the adsorption kinetics of EDTA and Eu^{III}-EDTA on COx clay rock. The results are given in the Supplementary data (Figs. S2 and S3). As in previously published studies, the adsorption kinetics did not help us to explain the main difference between batch and diffusion data, although they might explain the early break-through for experiments with shorter time-scales (<100 days). Similar conclusions were obtained on polymaleic acid percolation through COx clay rock by Durce et al. (2014). These authors included desorption kinetic and hysteresis in their model, which also failed to completely predict the percolation experiments.

Chemical perturbation of the rock and especially dissolution of minerals by EDTA is another assumption to consider (Golubev et al., 2006; Nowack and Sigg, 1997; Noren et al., 2009). It might enhance the organic flux from the upstream solution and the release of competing cations as well. Such a phenomenon was recently studied on limestone-shale saprolite (Mayes et al., 2000; Gwo et al., 2007). Interfacial chemical reactions led to a chemical mass transfer with a higher rate than the physical mass transfer. Co^{II}-EDTA was shown to be oxidised or dissociated on oxide surfaces, leading to Co^{III}-EDTA or Fe^{III}-EDTA respectively (Zachara et al., 1995). However, such dissociation processes were shown to be slow in COx clay rock and were ruled out by speciation measurements.

It would be worth carrying out further studies on these organic/sediments systems in order to quantify the accessible surface and site densities of various phases (and not only phyllosilicates) on crushed and compact samples.

6. Conclusion

This work discusses an original case study of metal-EDTA complex migration in a natural sedimentary rock. The adsorption of Eu^{III} was measured on COx clay rock as a function of [EDTA]. The predictive model based on the (Eu/COx and EDTA/COx) binary systems was in good agreement with results on the ternary system Eu/EDTA/COx. At low EDTA concentrations, Eu was mainly driven by Eu^{3+} adsorption and complexation by carbonates and EDTA. At higher EDTA concentrations, the behaviour of Eu^{III} was driven by the adsorption of the anionic complex $[Eu^{III}\text{-EDTA}]^-$ and less affected than EDTA by the saturation of adsorption sites. Thus Eu was used as a probe to quantify metal-EDTA transport. Time-resolved laser-induced fluorescence spectroscopy (TRLFS) confirmed that Eu^{III}EDTA was not quantitatively dissociated during diffusion. The adjusted effective diffusion coefficient, $D_e(Eu^{III}\text{-EDTA}) = 1.5–1.7 \cdot 10^{12}\ m^2\ s^{-1}$, was similar to previously published measurements ($D_e(^{14}C\text{-EDTA}) = 0.94\ \ 10^{12}\ m^2\ s^{-1}$), confirming anionic exclusion within the clay rock. Batch data and diffusion profiles in the rock confirmed the significant adsorption capacity of Callovo-Oxfordian clay rock, $R_d(Eu^{III}\text{-EDTA}) \sim 6–14\ L\ kg^{-1}$ leading to diffusive retardation. However, the diffusive retardation factors were lower than those predicted by the batch experiments by less than an order of magnitude ($2 < R_d^{BATCH}/K_d^{CELL} < 5$). This early break-through is consistent with most data on organic/soils organic/COx systems. Yet, it was contrary to the data obtained for EDTA on others rocks containing higher amounts of (hydr)oxides ($R_d/K_d < 1$). Improving our understanding of these systems will help us to define the relevant time and space scales needed to obtain consistent data from crushed and hard rocks. This would in turn improve our estimations of the confinement of hydrosoluble organic species in the geosphere.

Acknowledgments

In memory of Dr. Eric Giffaut, who was an immense support during these studies and spent many hours correcting the manuscript. This work received financial support from ANDRA. We would like to thank Aline Juery and Jonathan Klein for their help with the diffusion experiments. Thanks to Dr. A. Bacquin and to V. Blin for the graphical abstract and manuscript review. We would also like to thank Dr. C. Tournassat for help on the comparison between ^{152}Eu and Eu adsorption isotherms. The discussion was greatly improved thanks to comments from many reviewers.

Appendix A. Supplementary material

Supplementary data associated with this article can be found, in the online version, at http://dx.doi.org/10.1016/j.jhydrol.2016.11.014.

References

Alonso, U., Missana, T., García-Gutiérrez, M., Patelli, A., Siitari-Kauppi, M., Rigato, V., 2009. Diffusion coefficient measurements in consolidated clay by RBS micro-scale profiling. Appl. Clay Sci. 43, 477–484.

Alliot, C., Bion, L., Mercier, F., Toulhoat, P., 2006. Effect of aqueous acetic, oxalic, and carbonic acids on the adsorption of europium (III) onto α-alumina. J. Colloid Interface Sci. 298, 573–581.

ANDRA, 2005. Synthesis-evaluation of the feasibility of a geological repository in an argillaceous formation. <www.andra.fr>.

Bauer, T.A., Rabung, T., Claret, F., Schäfer, F., Buckau, G., Fanghänel, T., 2005. Influence of temperature on sorption of europium onto smectite: The role of organic contaminants. Appl. Clay Sci. 30, 1–10.

Bazer-Bachi, F., Tevissen, E., Descostes, M., Grenut, B., Meier, P., Simonnot, M.-O., Sardin, M., 2006. Characterization of iodide retention on Callovo-Oxfordian argillites and its influence on iodide migration. Phys. Chem. Earth, Parts A/B/C 31, 517–522.

Bazer-Bachi, F., Descostes, M., Tevissen, E., Meier, P., Grenut, B., Simonnot, M., Sardin, M., 2007. Characterization of sulphate sorption on Callovo-Oxfordian argillites by batch, column and through-diffusion experiments. Phys. Chem. Earth, Parts A/B/C 32, 552–558.

Borisover, M., Davis, J., 2015. Adsorption of inorganic and organic solutes by clay minerals. In: Tournassat, C., Steefel, C., Bourg, I.C., Bergaya, F. (Eds.), Natural and Engineered Clay Barriers. Elsevier.

Brooks, S.C., Taylor, D.L., Jardine, P.M., 1996. Reactive transport of EDTA-complexed cobalt in the presence of ferrihydrite. Geochim. Cosmochim. Acta 60 (11), 1899–1908.
Bruggeman, C., Liu, D.J., Maes, N., 2010. Influence of Boom Clay organic matter on the adsorption of Eu^{3+} by illite – geochemical modelling using the component additivity approach. Radiochim. Acta 98, 597–605.
Byegard, J., Skarnemark, G., Skalberg, M., 2000. Transport modelling of tracers influenced by kinetic hindered sorption – applied to laboratory and in situ studies of lanthanide EDTA complexes. J. Contam. Hydrol. 42, 165–186.
Crank, J., 1975. The Mathematics of Diffusion. Clarendron Press, London.
Dagnelie, R.V.H., Descostes, M., Pointeau, I., Klein, J., Grenut, B., Radwan, J., Lebeau, D., Georgin, D., Giffaut, E., 2014. Sorption and diffusion of organic acids through clayrock: comparison with inorganic anions. J. Hydrol. 511, 619–627.
Dagnelie, R.V.H., Arnoux, P., Radwan, J., Lebeau, D., Nerfie, P., Beaucaire, C., 2015. Perturbation induced by EDTA on HDO, Br- and EuIII diffusion in a large-scale clay rock sample. Appl. Clay Sci. 105–106, 142–149.
Darban, A.K., Foriero, A., Yong, R.N., 2000. Concentration effects of EDTA and chloride on the retention of trace metals in clays. Eng. Geol. 57, 81–94.
Descostes, M., Tevissen, E., 2004. Definition of an equilibration protocol for batch experiments on Callovo-Oxfordian argillite. Phys. Chem. Earth 29, 79–90.
Descostes, M., Blin, V., Bazer-Bachi, F., Meier, P., Grenut, B., Radwan, J., Schlegel, M.L., Buschaert, S., Coelho, D., Tevissen, E., 2008. Diffusion of anionic species in Callovo-Oxfordian argillites and Oxfordian limestones (Meuse/Haute-Marne, France). Appl. Geochem. 23, 655–677.
Durce, D., Landesman, C., Grambow, B., Ribet, S., Giffaut, E., 2014. Adsorption and transport of polymaleic acid on Callovo-Oxfordian clay stone: batch and transport experiments. J. Contam. Hydrol. 164, 308–322.
Gaucher, E., Robelin, C., Matray, J., Négrel, G., Gros, Y., Heitz, J., Vinsot, A., Rebours, H., Cassagnabère, A., Bouchet, A., 2004. ANDRA underground research laboratory: interpretation of the mineralogical and geochemical data acquired in the Callovian-Oxfordian formation by investigative drilling. Phys. Chem. Earth, Parts A/B/C 29, 55–77.
Giffaut, E., Grivé, M., Blanc, P., Vieillard, P., Colàs, E., Gailhanou, H., Gaboreau, S., Marty, N., Madé, B., Duro, L., 2014. Andra thermodynamic database for performance assessment: ThermoChimie. Appl. Geochem. 49, 225–236.
Golubev, S.V., Bauer, A., Pokrovsky, O.S., 2006. Effect of pH and organic ligands on the kinetics of smectite dissolution at 25 °C. Geochim. Cosmochim. Acta 70, 4436–4451.
Gwo, J.-P., Mayes, M.A., Jardine, P.M., 2007. Quantifying the physical and chemical mass transfer processes for the fate and transport of Co(II)EDTA in a partially-weathered limestone-shale saprolite. J. Contam. Hydrol. 90, 184–202.
Hummel, W., 2008. Radioactive contaminants in the subsurface: the influence of complexing ligands on trace metal speciation. Monatshefte für Chemie – Chem. Mon. 139, 459–480.
Kaplan, D.I., Serkiz, S.M., Allison, J.D., 2010. Europium sorption to sediments in the presence of natural organic matter: a laboratory and modeling study. Appl. Geochem. 25, 224–232.
Mayes, M.A., Jardine, P.M., Larsen, I.L., Brooks, S.C., Fendorf, S.E., 2000. Multispecies transport of metal-EDTA complexes and chromate through undisturbed columns of weathered fractured saprolite. J. Contam. Hydrol. 45, 243–265.
Menut, D., Fichet, P., Lacour, J., Rivoallan, A., Mauchien, P., 2003. Micro-laser-induced breakdown spectroscopy technique: a powerful method for performing quantitative surface mapping on conductive and nonconductive samples. Appl. Opt. 42.
Menut, D., Descostes, M., Meier, P., Radwan, J., Mauchien, P., Poinssot, C., 2005. Heavy metals migration in argilaceous rocks: on the use of micro laser-induced breakdown spectroscopy (micro LIBS) as a microanalysis tool. Scientific Basis Nucl. Waste Manage. XXIX 932, 913–918.
Moridis, G.J., 1998. A Set of semianalytical solutions for parameter estimation in diffusion cell experiments. Sci. York.
Noren, K., Loring, J.S., Bargar, J.R., Persson, P., 2009. Adsorption mechanisms of EDTA at the water-iron oxide interface: implications for dissolution. J. Phys. Chem. C 113, 7762–7771.
Nowack, B., Sigg, L., 1997. Dissolution of Fe(III) (hydr)oxides by metal-EDTA complexes. Geochim. Cosmochim. Acta 61, 951–963.
Pace, M.N., Mayes, M.A., Jardine, P.M., McKay, L.D., Yin, X.L., Mehlhorn, T.L., Liu, Q., Gürleyük, H., 2007. Transport of Sr^{2+} and $SrEDTA^{2-}$ in partially-saturated and heterogeneous sediments. J. Contam. Hydrol. 91, 267–287.
Parkhurst, D.L., Appelo, C.A.J., 1999. User's guide to PHREEQC (version 2) – a computer program for speciation, batch-reaction, one-dimensional transport, and inverse geochemical calculations. Water Resour. Invest. Rep., 99–4259
Pignatello, J.J., Xing, B., 1996. Mechanisms of slow sorption of organic chemicals to natural particles. Environ. Sci. Technol. 30, 1–11.
Rabung, T., Pierret, M., Bauer, A., Geckeis, H., Bradbury, M., Baeyens, B., 2005. Sorption of Eu(III)/Cm(III) on Ca-montmorillonite and Na-illite. Part 1: Batch sorption and time-resolved laser fluorescence spectroscopy experiments. Geochim. Cosmochim. Acta 69, 5393–5402.
Reinoso-Maset, E., Worsfold, P.J., Keith-roach, M.J., 2012. The effect of EDTA, NTA and picolinic acid on Th(IV) mobility in a ternary system with natural sand. Environ. Pollut. 162, 399–405.
Roberts, P.V., Goltz, M.N., Mackay, D.M., 1986. 3. Retardation estimates and mass balances for organic solutes. Water Resour. Res. 22, 2047–2058.
Schaffer, M., Licha, T., 2015. A framework for assessing the retardation of molecules in groundwater: implications of the species distribution for the sorption-influenced transport. Sci. Total Environ. 524–525, 187–194.
Seliman, A.F., Borai, E.H., Lasheen, Y.F., Abo-Aly, M.M., DeVol, T.A., Powell, B.A., 2010. Mobility of radionuclides in soil/groundwater system: comparing the influence of EDTA and four of its degradation products. Environ. Pollut. 158, 3077–3084.
Szecsody, J.E., Zachara, J.M., Bruckhart, P.L., 1994. Adsorption-dissolution reactions affecting the distribution and stability of Co^{II}EDTA in iron oxide-coated sand. Environ. Sci. Technol. 28, 1706–1716.
Szecsody, J.E., Zachara, J.M., Chilakapati, A., Jardine, P.M., Ferrency, A.S., 1998. Importance of flow and particle-scale heterogeneity on $Co^{II/III}$ EDTA reactive transport. J. Hydrol. 209, 112–136.
Tebes-stevens, C., Valocchi, A.J., Vanbriesen, J.M., Rittmann, B.E., 1998. Multicomponent transport with coupled geochemical and microbiological reactions: model description and example simulations. J. Hydrol. 209, 8–26.
Tertre, E., Berger, G., Simoni, E., Castet, S., Giffaut, E., Loubet, M., Catalette, H., 2006. Europium retention onto clay minerals from 25 to 150 °C: experimental measurements, spectroscopic features and sorption modelling. Geochim. Cosmochim. Acta 70, 4563–4578.
Tits, J., Wieland, E., Bradbury, M.H., 2005. The effect of isosaccharinic acid and gluconic acid on the retention of Eu (III), Am (III) and Th (IV) by calcite. Appl. Geochem. 20, 2082–2096.
Wang, Z.-M., van de Burgt, L.J., Choppin, G.R., 2000. Spectroscopic study of lanthanide(III) complexes with aliphatic dicarboxylic acids. Inorgan. Chim. Acta 310, 248–256.
Weber Jr., W.J., McGinley, P.M., Katz, Lynn, E., 1991. Sorption phenomena in subsurface systems: concepts, models and effect on contaminant fate and transport. Water Res. 25, 499–528.
Wu, S.L., Horrocks, W.D., 1996. General method for the determination of stability constants of lanthanide ion chelates by ligand-ligand competition: laser-excited Eu^{3+} luminescence excitation spectroscopy. Anal. Chem., 394–401
Xie, F., Zhang, T.A., Dreisinger, D., Doyle, F., 2014. A critical review on solvent extraction of rare earths from aqueous solutions. Miner. Eng. 56, 10–28.
Zachara, J.M., Gassman, P.L., Smith, S.C., Taylor, D., 1995. Oxidation and adsorption of Co(II) $EDTA^{2-}$ complexes in subsurface materials with iron and manganese oxide grain coatings. Geochim. Cosmochim. Acta 59, 4449–4463.